Functional replacement of isoprenoid pathways in *Rhodobacter sphaeroides*

Enrico Orsi,[1],[†] [iD] Jules Beekwilder,[2],[†]
Dewi van Gelder,[1] Adèle van Houwelingen,[2]
Gerrit Eggink,[1],[3] Servé W.M. Kengen[4] and
Ruud A. Weusthuis[1]*

[1]*Bioprocess Engineering, Wageningen University,
6708PB Wageningen, The Netherlands.*
[2]*Wageningen Plant Research, 6700AA Wageningen,
The Netherlands.*
[3]*Wageningen Food and Biobased Research, 6708WG
Wageningen, The Netherlands.*
[4]*Laboratory of Microbiology, Wageningen University,
6708WE Wageningen, The Netherlands.*

Summary

Advances in synthetic biology and metabolic engineering have proven the potential of introducing metabolic by-passes within cell factories. These pathways can provide a more efficient alternative to endogenous counterparts due to their insensitivity to host's regulatory mechanisms. In this work, we replaced the endogenous essential 2-C-methyl-D-erythritol 4-phosphate (MEP) pathway for isoprenoid biosynthesis in the industrially relevant bacterium *Rhodobacter sphaeroides* by an orthogonal metabolic route. The native 2-C-methyl-D-erythritol 4-phosphate (MEP) pathway was successfully replaced by a heterologous mevalonate (MVA) pathway from a related bacterium. The functional replacement was confirmed by analysis of the reporter molecule amorpha-4,11-diene after cultivation with [4-^{13}C]glucose. The engineered *R. sphaeroides* strain relying exclusively on the MVA pathway was completely functional in conditions for sesquiterpene production and, upon increased expression of the MVA enzymes, it reached even higher sesquiterpene yields than the control strain coexpressing both MEP and MVA modules. This work represents an example where substitution of an essential biochemical pathway by an alternative, heterologous pathway leads to enhanced biosynthetic performance.

Introduction

Synthetic biology conceptualizes biological functions as independent parts which can be manipulated and whose effects can be analysed (Benner and Sismour, 2005). Applying this view to cellular metabolism, the metabolic network of a microorganism can be divided into metabolic pathways (modules resembling operation units) which can be modelled and optimized (Stephanopoulos, 2012). Engineering *modules* as parts of *wholes* (Stephanopoulos, 2012; Kendig and Eckdahl, 2017) are an expression that suggests the interchangeability of parts within biological systems, which can still result in functional organisms. Application of this concept allowed to achieve remarkable results in terms of metabolic optimization for a wide range of biotechnological applications (Ajikumar *et al.*, 2010; Bonacci *et al.*, 2012; Wu *et al.*, 2013; Zhou *et al.*, 2015; Jiang *et al.*, 2017).

Isoprenoid biosynthesis provides an example of 'natural' independence between essential modules. In nature exist two essentially different biosynthetic routes which branch from the central metabolism and converge to the isoprene units isopentenyl-diphosphate (IPP) and dimethylallyl-diphosphate (DMAPP). These are the 2-C-methyl-D-erythritol 4-phosphate (MEP) and the mevalonate (MVA) pathway. With few exceptions, they are generally phylogenetically distinct, with MEP being present in prokaryotes, and MVA in eukaryotes and archaea. Photosynthetic eukaryotes harbour both pathways naturally, compartmentalizing the MEP pathway within the chloroplast while the MVA pathway operates in the cytosol (Vranová *et al.*, 2013). The MEP pathway starts with the condensation of glyceraldehyde-3-phosphate (GAP) with pyruvate (PYR), while the MVA pathway uses acetoacetyl-CoA (AA-CoA) and acetyl-CoA (Ac-CoA) as substrates. The products of the two pathways, IPP and its isomer DMAPP, are the starting compounds for all terpenoids (Grünler *et al.*, 1994). These compounds are essential for the organism, as they are involved in several functions necessary for life, like

respiration and photosynthesis by ubiquinone, chlorophyll and carotenoids respectively. Moreover, many terpenoids have raised interest in biotechnology as interesting compounds for pharmaceutical, flavours, chemicals and also biofuels (Ajikumar *et al.*, 2008; Peralta-Yahya *et al.*, 2012; Liao *et al.*, 2016; Mewalal *et al.*, 2016; Niu *et al.*, 2017; Schempp *et al.*, 2017).

Biotechnological production of terpenoids by engineered microbial cell factories (or *chassis*) has been extensively described, coexpressing both MEP and MVA pathways together, mainly for bypassing the regulation on the host's native biosynthetic route (Withers and Keasling, 2007; Zurbriggen *et al.*, 2012). An example of organism that has undergone this type of engineering is *Rhodobacter sphaeroides* (Beekwilder *et al.*, 2014). In fact, this bacterium is raising interest as potential platform for biotechnological isoprenoid production. In this species, low oxygen conditions lead to formation of intracellular membranes rich of isoprenoid-derived compounds like carotenoids and bacteriochlorophylls. Moreover, several studies have been performed for exploiting this microorganism for the production of coenzyme Q_{10} and sesquiterpenes (Beekwilder *et al.*, 2014; Lu *et al.*, 2015; Orsi *et al.*, 2019).

Here, the effect of fully replacing the native MEP pathway by a heterologous MVA pathway is described for *R. sphaeroides*. The resulting microorganism relies exclusively on the MVA pathway and produces sesquiterpenes at an even higher yield than the parental strain harbouring both MEP and MVA pathways. This work represents an example of replacement of an essential pathway by an independent module, resulting in an improvement of the metabolic capacities of a *chassis*.

Results and discussion

Strategy for isoprenoid pathway replacement

Substitution of an endogenous pathway by an independent and heterologous alternative requires inactivation of the former, while including all the information needed for the functioning of the latter. In *R. sphaeroides*, the MEP pathway connects GAP and PYR to IPP and DMAPP via 7 enzymatic steps. Additionally, it requires at least two types of cofactors for its activity, which are NADPH and flavodoxin or ferredoxin (Fig. 1A). On the other hand, the MVA pathway consists of six enzymatic reactions that link AA-CoA to IPP and DMAPP. Different from the MEP pathway, the only cofactor required by the MVA pathway is NADPH (Fig. 1A). Therefore, replacement of the isoprenoid pathway in this species should be feasible by just combining MEP inactivation to MVA introduction. Other authors suggested the possibility of substituting the native MEP pathway by autonomous bypasses towards IPP and DMAPP (Puan *et al.*, 2005;

Loiseau *et al.*, 2007; Kirby *et al.*, 2015; Chatzivasileiou *et al.*, 2019). Nevertheless, in all these cases the non-native routes implemented required additional carbon sources for their functioning (e.g. mevalonate or isoprenol), leading to auxotrophic organisms, whose growth was dependent on a two-substrate cultivation system. Only under this condition, the engineered microorganisms were able to grow and synthesize isoprenoids, often with important growth deficits (Chatzivasileiou *et al.*, 2019). Conversely, the goal of our design is to replace the isoprenoid pathway without interfering with the rest of the host's metabolism.

The most obvious approach for MEP pathway deletion would be targeting the first enzyme branching from the central metabolism, 1-deoxy-D-xylulose 5-phosphate synthase (Dxs). However, this strategy has two disadvantages. First, the product of Dxs, 1-deoxy-D-xylulose 5-phosphate (DXP) is required for thiamine biosynthesis (Fig. 1A). Second, recently discovered metabolic pathways could in principle still generate DXP in case of Dxs deletion. These are the 5'-methylthioadenosine-isoprenoid shunt (Erb *et al.*, 2012) and the putative route from pentose phosphates to DXP (Kirby *et al.*, 2015). Therefore, we considered to inactivate the second enzyme of the MEP pathway, 1-deoxy-D-xylulose 5-phosphate reductoisomerase, Dxr. This enzyme is not known to be involved in other biosynthetic processes. The operon including *dxr* contains genes required for cellular growth and proliferation (Fig. 1B, Table S3). Aiming not to affect the expression of the genes downstream of *dxr*, a clean knockout with the removal of 1188 bp on the *dxr* locus was proposed. For this purpose, two pBBR_Cas9_*Δdxr* plasmids were constructed, each one containing a different targeting spacer (sp1, sp2, Table S4, Fig. S1).

To assess the likeliness of a reverse flux from IPP via the MEP pathway as result of *dxr* inactivation, we calculated (Flamholz *et al.*, 2012) the Gibbs free energies of the two pathways (Table S5). The last step of the native isoprenoid pathway catalysed by 4-hydroxy-3-methylbut-2-enyl diphosphate (HMBPP) reductase (IspH) has a highly negative $\Delta_r G'^0$ (-62.5 ± 6.4 kJ mol^{-1}) (Fig. 1A). Therefore, reverse flux via the MEP pathway is not expected to occur at any situation.

Introduction of a functional MVA pathway requires the harmonious expression of 6 different genes. Previous work demonstrated the possibility of integrating an MVA pathway in the genome of a photosynthetic microorganism (Bentley *et al.,* 2014). Phylogenetically, the traditional distinction that couples MEP pathway to the prokaryotic domain and MVA to eukaryotes and archaea has been revised (Lombard and Moreira, 2011). The α-proteobacterium *Paracoccus zeaxanthinifaciens* (Hümbelin *et al.*, 2002) harbours a complete MVA pathway, with all required genes organized in an operon.
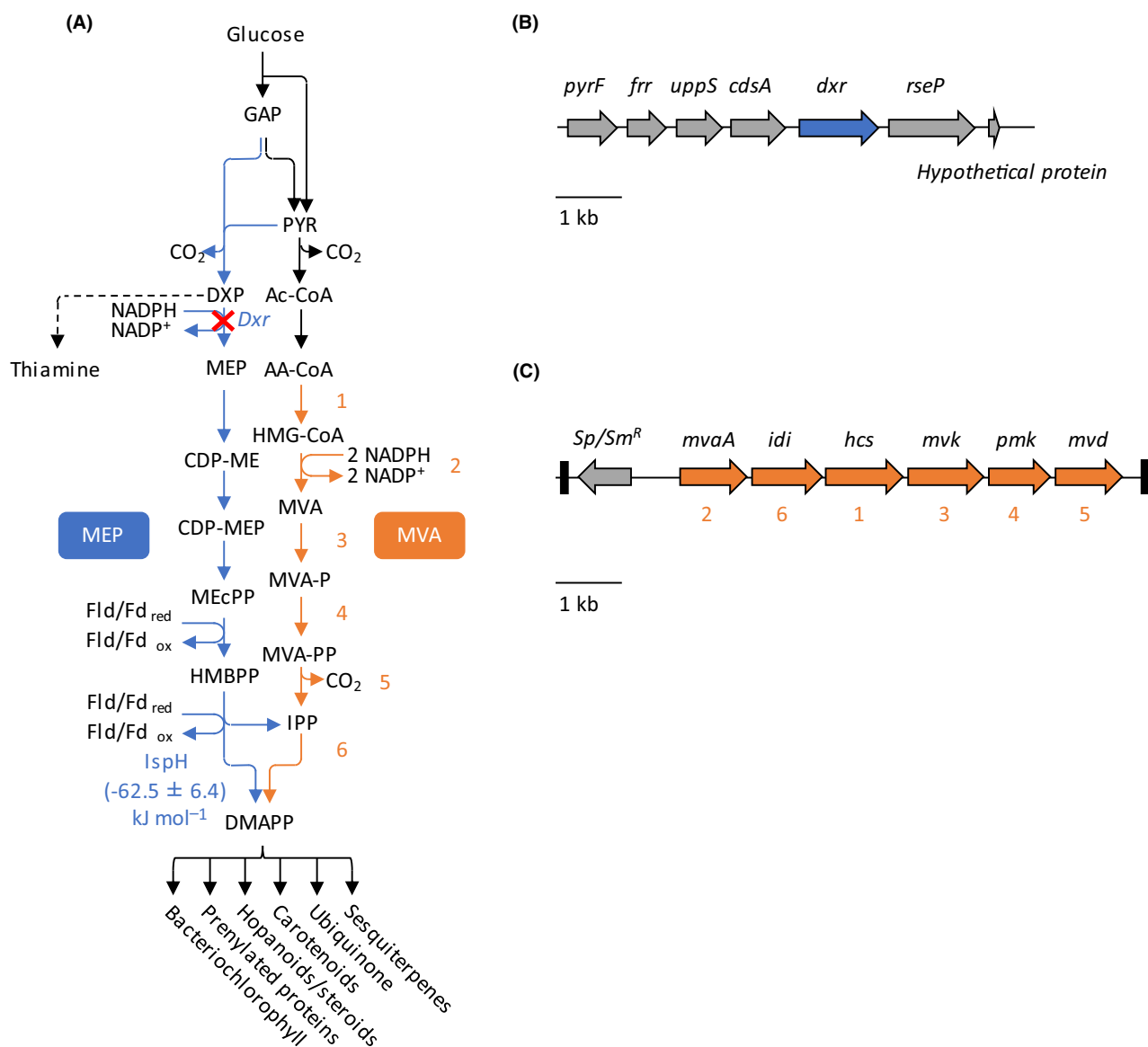
Fig. 1. Overview of the strategy for isoprenoid pathway replacement in *Rhodobacter sphaeroides*.

A. representation of the two isoprenoid modules 2-C-methyl-D-erythritol 4-phosphate (MEP, blue arrows) and mevalonate (MVA, orange arrows). Both modules branch from the central metabolism (black arrows) and converge to isopentenyl-diphosphate (IPP) and dimethylallyl-diphosphate (DMAPP), which are the precursors of all terpenoids (some listed below DMAPP). MVA pathway requires NADPH as cofactor, while the endogenous MEP additionally requires reduced flavodoxin (Fld) or ferredoxin (Fd) for its functioning (red: reduced, ox: oxidized). The proposed position for inactivation of the native MEP pathway is also shown and corresponds to the enzyme 1-deoxy-D-xylulose 5-phosphate reductoisomerase (Dxr, red cross). Its substrate 1-deoxy-D-xylulose 5-phosphate (DXP) is also involved in thiamine biosynthesis (black dashed line). The last step of the MEP pathway is catalysed by 4-hydroxy-3-methylbut-2-enyl diphosphate (HMBPP) reductase (IspH). For this enzyme, the Gibbs free energy under standard conditions was calculated (in blue). The highly negative $\Delta_r G'^0$ of the reaction (-62.5 ± 6.4 kJ mol^{-1}) indicates irreversibility of its enzymatic activity. On the other hand, introduction of the MVA module requires the correct functioning of 6 enzymes (numbered in orange).

B. overview of the operon including the target gene *dxr*. All the other genes included are involved in growth-related functions (see Table S3 for more information).

C. overview of the MVA operon from the α-proteobacterium *Paracoccus zeaxanthinifaciens* used for integration via mini transposon system pUT-Mini-Tn5-Sp/Sm. The numbers below the genes represent their position in the pathway depicted in panel A), while Sp/Sm^R refers to spectinomycin/streptomycin resistance. The image is adapted from (Hümbelin *et al.*, 2002). Other abbreviations: GAP (glyceraldehyde-3-phosphate), PYR (pyruvate), CDP-ME (4-(cytidine 5'-diphospho)-2-C-methyl-D-erythritol), CDP-MEP (2-phospho-4-(cytidine 5'-diphospho)-2-C-methyl-D-erythritol), MEcPP (2-C-methyl-D-erythritol 2,4-cyclodiphosphate), pyrF (uridylate kinase, gene), frr (ribosome recycling factor, gene), uppS (undecaprenyl-diphosphate synthase, gene), cdsA (phosphatidate cytidylyltransferase, gene), rseP (Regulator of sigma E protease, gene) Ac-CoA (acetyl-CoA), AA-CoA (acetoacetyl-CoA), HMG-CoA (S)-3-hydroxy-3-methylglutaryl-CoA), MVA-P ((R)-5-phosphomevalonate), MVA-PP ((R)-5-diphosphomevalonate), mvaA (HMG-CoA reductase, gene), idi (IPP isomerase, gene), hcs (HMG-CoA synthase, gene), mvk (mevalonate kinase, gene), pmk (phosphomevalonate kinase, gene), mvd (MVA-PP decarboxylase, gene).

This operon already proved to be functional when expressed on a replicative plasmid in *R. sphaeroides* (Beekwilder *et al.*, 2014). Therefore, the MVA operon from *P. zeaxanthinifaciens* was chosen for genomic integration and cloned into a mini Tn5 transposon system harbouring spectinomycin resistance (Fig. 1C). Two reporter genes were used to determine the effect of the heterologous pathway on sesquiterpene production: valencene synthase and amorpha-4, 11-diene synthase (Beekwilder *et al.*, 2014; Orsi *et al.*, 2019).

Replacement of isoprenoid pathways

A first attempt to delete *dxr* was performed on a wild-type strain of *R. sphaeroides* (Rs265). The number of colonies obtained after conjugation was very low (< 10 in a plate with 10^{-2} dilution). They revealed to be all *wt* genotypes, indicating that isoprene synthesis is essential for cell survival. Therefore, an alternative strategy was adopted, which consisted in first integrating the MVA module by transposon insertion, followed by MEP inactivation. For this purpose, a strain harbouring the valencene synthase gene (Rs265 + pBBR-CnVS) (Beekwilder *et al.*, 2014) was chosen. The MVA pathway was successfully introduced into the *R. sphaeroides* genome by transposition. Fifteen independent transposition events were tested for valencene production. For all the Rs265-MVA strains, an increase of $\pm$ 1.5 times compared with the Rs265 control strain was observed (Fig. 2A). This indicates that multiple integration sites within the *R. sphaeroides* genome could equally support expression and functionality of the heterologous MVA pathway (Fig. 2A).

After confirmation of the MVA operon integration, *dxr* inactivation was followed. Indeed, *dxr* knockout colonies were obtained. This result indicated that at least under plate conditions, it is possible to successfully replace the native MEP pathway by the MVA pathway (Fig. S2). Here, the number of conjugants obtained was two orders of magnitude higher than for the Rs265, and resulted in a high efficiency of *dxr* deletion (*Δdxr*), independently from the spacer used. In fact, Cas9 counter-selection with both spacers showed a high success rate, with 98% and 77% of deletions obtained for sp1 and sp2 respectively (Table S6). Therefore, due to the essentiality of isoprenoids for cellular anabolism and homeostasis (Kirby and Keasling, 2009), inactivation of the native MEP module was possible only after integration of the heterologous MVA pathway.

Quantitative physiological characterization after functional pathway replacement

The resulting Rs265-MVA-*Δdxr* strain with integrated MVA and inactivated MEP pathway was cured from the pBBR-CnVS plasmid, and subsequently conjugated with the pBBR-*ads* plasmid harbouring the amorpha-4,11-diene synthase gene. Cultivation of this strain showed similar growth rates to the parental strains relying on the native MEP pathway (Rs265) or on the coexpression between MEP and MVA (Rs265-MVA) (Fig. 2B, Fig. S3 and S4). Moreover, the biomass concentration obtained after 24 h incubation was comparable to the one of the two parental strains (Fig. 2C). Thus, the Rs265-MVA-*Δdxr* strain can efficiently and exclusively rely on the integrated MVA module for its functioning. In addition to growth measurements, final amorphadiene titres were measured for three different biological replicates of Rs265-MVA-*Δdxr* (#5, 6 and 7), and compared with Rs265-MVA and Rs265 strains (Fig. 2D). The resulting values indicate that while the coexpression of MEP and MVA increased amorphadiene titres of about 1.2-fold, inactivation of the MEP pathway resulted in a decrease of about threefold. A similar assessment was performed on endogenous terpenoids, including carotenoids, coenzyme Q_{10} and bacteriochlorophyll (Fig. 3). Also for these compounds, replacement of MEP with the MVA module leads to a decrease in relative abundances for Rs265-MVA-*Δdxr* between two- and fivefold compared with Rs265. This suggests that although efficiently supporting growth, the integrated MVA pathway carries a lower flux towards IPP and DMAPP compared with the endogenous MEP pathway (Fig. 2D).

Previous works tried to achieve the same functional replacement of isoprenoid pathways by expressing a bacterial MEP pathway in *Saccharomyces cerevisiae* while inactivating the native MVA metabolic route (Partow *et al.*, 2012; Carlsen *et al.*, 2013; Kirby *et al.*, 2016). In all cases, the pathway replacement was inefficient or suboptimal, suggesting insufficient complementation of the detrimental effect associated to endogenous MVA inactivation. As reported by the authors, the last two steps of the MEP pathway catalysed by IspG and IspH rely on [4Fe-4S] clusters and on cytosolic ferredoxin and/or flavodoxin (the latter non-native in *S. cerevisiae*). Moreover, assembly of these clusters requires a specific iron–sulphur cluster (ISC) machinery, which is not native in *S. cerevisiae*. A more recent approach (Kirby *et al.*, 2016) involved a screening of natural IspG and IspH homologs. Combined with selection and engineering of heterologous redox partners and of ISC machinery, this approach led to a functionally integrated MEP pathway, as shown by ^{13}C cultivation. Nevertheless, inactivation of the MVA pathway resulted in suboptimal growth of the mutant, which could moderately grow exclusively under a low aeration range and only by previous supply of mevalonate in the preculture stage on plate (Kirby *et al.*, 2016). In this work, possibly, the lack of non-native metal-clusters and cofactors required for the MVA
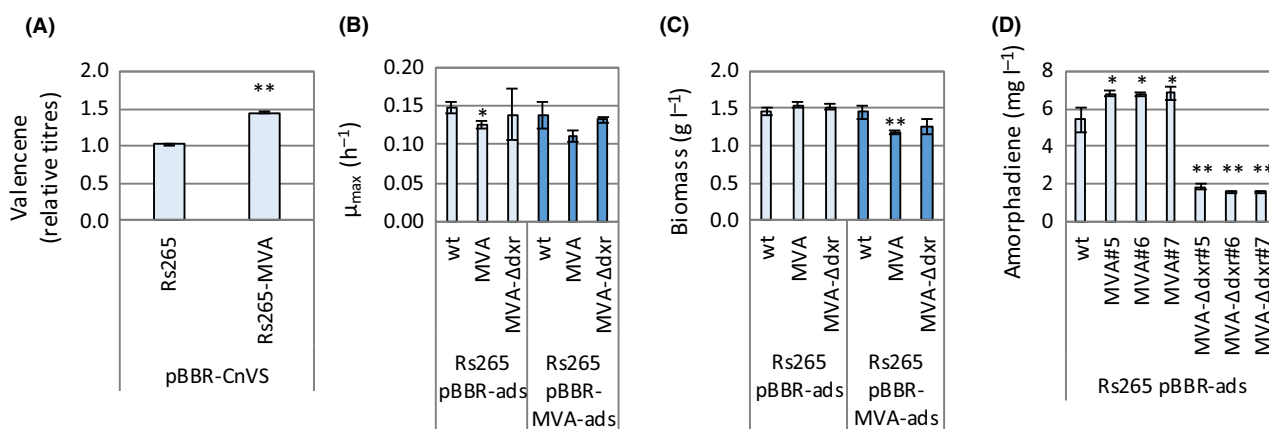
Fig. 2. Effect of isoprenoid pathways replacement on physiological parameters in *Rhodobacter sphaeroides*. Comparison of (A) relative valencene titres between Rs265 + pBBR-CnVs and the average of 15 biological replicates Rs265-MVA + pBBR-CnVS obtained after transposon insertion of the MVA operon. Bars show the average between the replicates ± SD of the replicates. Comparison of (B) growth rates and (C) biomass concentration after 24 h cultivation on defined medium. The Rs265 strains tested are wild type (wt), integrated mevalonate (MVA) and Δ*dxr* on MVA integrated background (MVA-Δ*dxr*). Strains were tested before and after the addition of extra copies of the MVA module on a plasmid (pBBR-*ads*, light blue and pBBR-MVA-*ads*, dark blue).

(D) Effect of MVA pathway integration and 2-C-methyl-D-erythritol 4-phosphate (MEP) pathway inactivation on amorphadiene titres. The strains tested were incubated for 24 h, and amorphadiene was measured at the end of the cultivation. The measurement includes the biological replicates 5, 6 and 7 obtained after transposon insertion of the MVA pathway (panel a). As for (B) and (C), also here the wt strain was compared with strains coexpressing isoprenoid modules (MVA) or the MVA module exclusively (MVA-Δ*dxr*). Unless expressed differently, the error bars are obtained from averages between at least biological triplicates. Significant differences are marked by either one or two asterisks (*$P < 0.05$, **$P < 0.01$). They were evaluated by comparing the set of replicates for the mutants Rs265-MVA (MVA) and Rs265-MVA-Δ*dxr* (MVA-Δ*dxr*) to the replicates obtained by the Rs265 (wt) strain by means of Student's *t*-test.
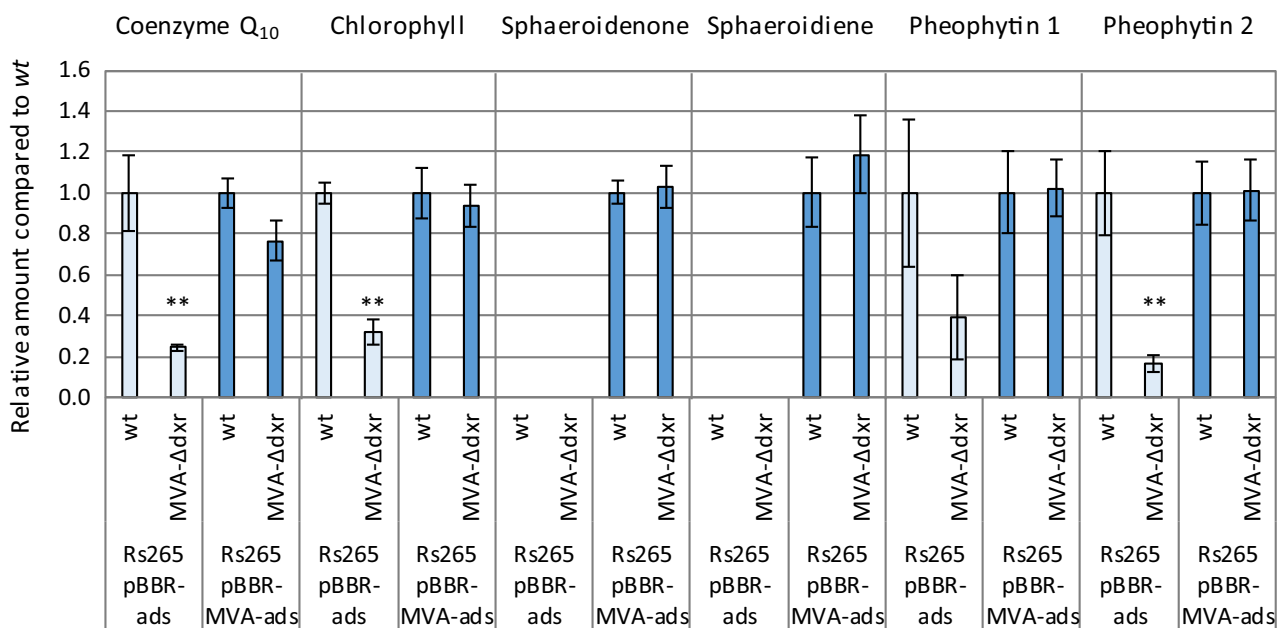

Fig. 3. Effect of isoprenoid pathways replacement on biosynthesis of endogenous terpenoids. Accumulation of endogenous terpenoids in *Rhodobacter sphaeroides* Rs265 relying exclusively on the native MEP pathway (wt), or on the heterologous mevalonate pathway (MVA-Δ*dxr*). The values represent the relative comparisons of MVA-Δ*dxr* to the wt control for several endogenous terpenoids (mentioned above each chart). Both MVA-Δ*dxr* and wt genotypes were tested before and after the addition of extra copies of the MVA module on a multicopy plasmid (pBBR-*ads*, light blue, and pBBR-MVA-*ads*, dark blue). Titres were measured after 24 h incubation on defined medium supplied with glucose. Errors represent the standard deviations between biological triplicates. Significant differences are marked by two asterisks (**$P < 0.01$). They were evaluated by comparing the set of replicates for the mutants Rs265-MVA-Δ*dxr* to the replicates obtained by the Rs265 (wt) strain by means of Student's *t*-test.

pathway enabled its complete functional expression in *R. sphaeroides*.

Confirmation of pathway replacement by ^{13}C analysis

To the genetic evidence of *dxr* inactivation (Fig. S2), phenotypic demonstration of isoprenoid biosynthesis exclusively via the MVA module was followed. To further confirm the lack of a catalytically active MEP pathway, we performed ^{13}C-cultivations with strain Rs265-MVA-*Δdxr* + pBBR-*ads* and compared them to strains Rs265 + pBBR-*ads* and Rs265-MVA + pBBR-*ads*. The strains were cultivated with defined medium supplied with [4-^{13}C]glucose as only carbon source. By using this substrate (Fig. 4A), isopentenyl-diphosphate (IPP) originating from the MEP pathway will maintain the ^{13}C atom in its backbone, which eventually will be incorporated into the reporter sesquiterpene amorphadiene (Orsi *et al.*, 2020). In contrast, the ^{13}C atom will be lost in the MVA pathway, as CO_2 is released in the conversion of pyruvate to acetyl-CoA, which precedes the entry point of the orthogonal pathway (Fig. 4A). After 24 h of cultivation, the mass distribution of amorphadiene was analysed by GC-MS. The three strains (Fig. 4B) showed clearly different mass distribution patterns. In the Rs265 + pBBR-*ads* strain, amorphadiene was generated exclusively from a pool of IPPs synthesized by the MEP pathway, as evidenced by the major peak of mass m/z M + 3. In the strain Rs265-MVA + pBBR-*ads* with the integrated MVA pathway, IPP can be synthesized by both MEP and MVA pathways, and consequently both labelled and unlabelled IPPs will be incorporated into amorphadiene. As a result, amorphadiene molecules of mass M and M + 1 are detected in equal amounts. Accordingly, in the strain Rs265-MVA-*Δdxr* + pBBR-*ads* yielded mostly unlabelled amorphadiene, as was also observed in the control cultivation with unlabelled [^{12}C] glucose using Rs265 + pBBR-*ads*. In both cases, the peak of unlabelled amorphadiene was higher than 80% (Fig. 4B). The frequency of ∼ 15–18% of the M + 1 fraction originates from the natural occurrence of ^{13}C atoms (∼ 1%), which randomly incorporated in one of the 15 atoms of amorphadiene ($C_{15}H_{24}$). Therefore, the isotope profile of the secreted reporter molecule amorphadiene confirmed that the isoprenoid flux via the MEP pathway was completely replaced by the MVA pathway in the Rs265-MVA-*Δdxr* + pBBR-*ads* strain.

Overexpression of the MVA module allows maximal isoprenoid biosynthesis in the Rs265-MVA-*Δdxr* strain

The Rs265-MVA-*Δdxr* strain synthesizes isoprenoid exclusively via the non-native MVA module (Fig. 4B). Clearly, the single MVA copy integrated in the genome

showed limited capacity for supporting biosynthesis of both endogenous and heterologous isoprenoids (Fig. 2D). To enhance the flux through the MVA pathway, the Rs265-MVA-*Δdxr* strain was conjugated with the multicopy pBBR-MVA-*ads* plasmid, which expresses an extra copy of the MVA module. The growth parameters of this strain did not differ from the parental Rs265 + pBBR-MVA-*ads* (Fig. 2B, C, Table S7, Fig. S4). Moreover, enhanced expression of the MVA pathway restored biosynthesis of the endogenous terpenoids in Rs265-MVA-*Δdxr* to levels that are not significantly different from the Rs265 + pBBR-MVA-*ads* strain (Fig. 3). Surprisingly, the Rs265-MVA + pBBR-MVA-*ads* strain (with the integrated MVA operon, the plasmid-born MVA enzymes copies and a still catalytically active MEP pathway) showed a slightly lower growth rate compared with the other two strains (Fig. 2B), and resulted in a lower final biomass concentration (Fig. 2C). This could indicate a possible burden in this strain due to the augmented expression levels of the MVA pathway.

The main advantage of harnessing non-endogenous and autonomous pathways for metabolic engineering purposes is the bypass of host's native regulation mechanisms (Liu *et al.*, 2018). We assessed this principle by determining the effect of extra copies of the MVA module in the presence and absence of the endogenous MEP pathway. Therefore, we determined the effect of increased MVA expression in terms of amorphadiene yield on glucose. This value was compared between the two strains harbouring the integrated MVA operon. These are the Rs265-MVA-*Δdxr* and the Rs265-MVA strains, with the latter still maintaining a functional MEP pathway. For both strains, augmentation in expression of the MVA pathway due to the pBBR-MVA-*ads* plasmid resulted in an increase in amorphadiene yield (Fig. 5). Remarkably, the effect on the Rs265-MVA-*Δdxr* strains was much more pronounced than for the Rs265-MVA strain, reaching a final yield of about 8 mg g^{-1} glucose (Rs265-MVA-*Δdxr*), while for the parental strain (Rs265-MVA), the yield approached a value of only 4 mg g^{-1} glucose. In terms of relative yield increase, this means up to 18-fold increase for the Rs265-MVA-*Δdxr* strain, while it limits to a value of 2.5-fold for the parental Rs-MVA strain (Fig. 5). This important increase for the Rs265-MVA-*Δdxr* strain persisted independently in all three biological replicates tested (Fig. 5), confirming to be independent from the genomic location of the MVA operon integration.

These results suggested that the augmented MVA capacity could be exploited at full potential when the MEP pathway was inactivated, resulting in a higher flux towards IPP compared with the strain coexpressing both MEP and MVA modules. Apparently, the MVA pathway can be affected by the endogenous MEP pathway when
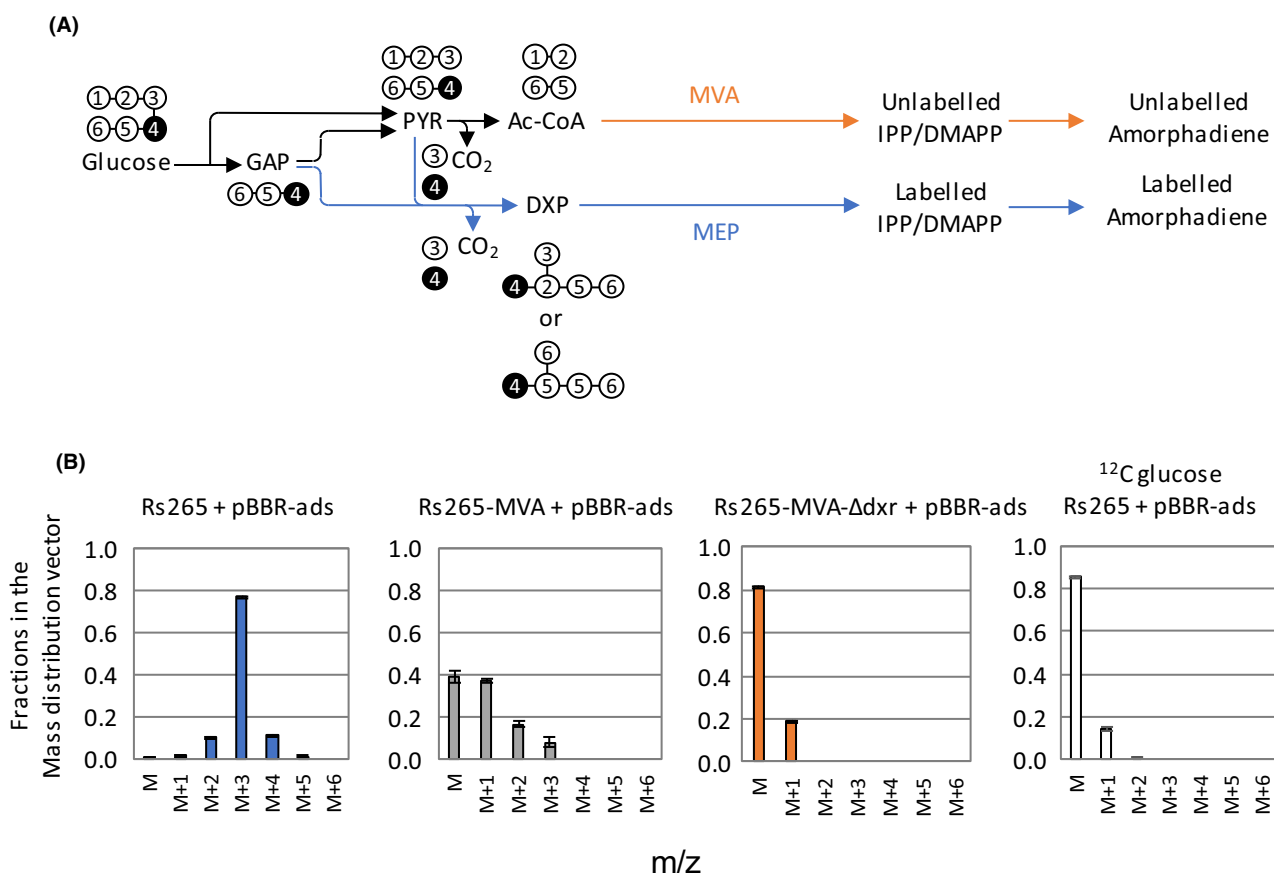
(A)

(B)

m/z

Fig. 4. Comparison of amorphadiene mass distribution vectors (MDVs) after [4^{13}C]glucose cultivation (A) Schematic representation of ^{13}C atoms incorporation in amorphadiene after [4-^{13}C]glucose cultivation. Glycolysis in *Rhodobacter sphaeroides* will generate 1 molecule of glyceraldehyde-3-phosphate (GAP) and 1 molecule of pyruvate (PYR) per glucose consumed. Additionally, GAP can be converted to PYR by the lower glycolysis. In case of isopentenyl-pyrophosphate (IPP) biosynthesis via the MEP pathway, the ^{13}C atom from GAP will be maintained within the carbon backbone. Differently, when PYR is converted to acetyl-CoA (Ac-CoA), the decarboxylation step results in ^{13}C atom removal from the carbon skeleton. Therefore, the IPP and dimethylallyl-diphosphate (DMAPP) molecules generated via the MVA pathway will be unlabelled, whereas they will maintain the ^{13}C atom if generated from MEP. Eventually, three molecules of IPP and DMAPP are condensed in one molecule of amorphadiene, whose isotopes spectra will be analysed by GC-MS.
B. Qualitative comparison between the MDVs of the secreted amorphadiene after [4-^{13}C]glucose cultivation. Due to the presence of three labelled IPP/DMAPP units, the strain exclusively expressing the MEP pathway (Rs265 + pBBR-*ads*) shows the highest density of ^{13}C incorporation within its backbone as a shift of M + 3 in m/z. The relative amount of ^{13}C within amorphadiene decreases when the two modules are coexpressed due to the presence of unlabelled IPP/DMAPP units in amorphadiene (Rs265-MVA + pBBR-*ads*). Eventually, the amount of ^{13}C incorporated when only MVA is active (Rs265-MVA-*Δdxr* + pBBR-*ads*) equals the natural distribution of ^{13}C that is incorporated by a strain relying on MEP exclusively grown on [^{12}C]glucose (white bars). Error bars represent the standard deviation of biological triplicates.

still active, as already shown for Rs265-MVA + pBBR-MVA-*ads* (Fig. 2B, C). Hence, exclusive use of the heterologous MVA module holds promising potential for biotechnological production of relevant isoprenoid compounds in *R. sphaeroides*.

In addition, our data indicate the existence of an interaction between MEP and MVA pathways, which limited the increase in amorphadiene yield in the Rs265-MVA + pBBR-MVA-*ads* strain. Further research by metabolomics or ^{13}C metabolic flux analysis could help in unravelling the nature of the interaction between these two metabolic pathways.

Conclusions

In this work we showed that in *R. sphaeroides*, the essential pathway for isoprenoid biosynthesis can be functionally replaced by an alternative, heterologous pathway, without penalty on growth or isoprenoid production capacity. Overexpression of the non-native MVA pathway enzymes allowed to achieve similar endogenous membrane-bound terpenoids titres compared with the control strain. Moreover, overexpression of the MVA module had much larger effects on heterologous sesquiterpene titres when the endogenous MEP pathway
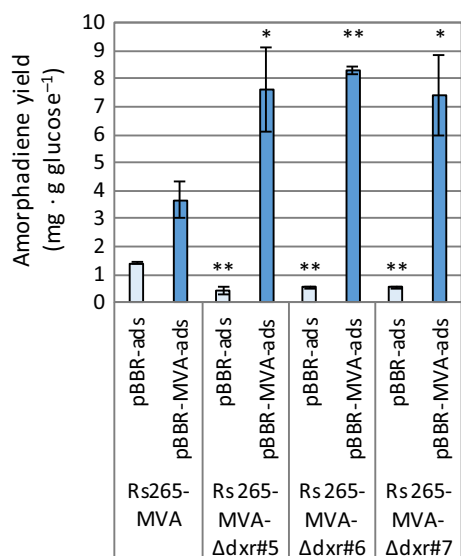
Fig. 5. Effect of increasing enzyme copies of the MVA module on amorphadiene yield. Comparison of amorphadiene yields on glucose after 24 h incubation on defined medium. The parental strain coexpressing the native endogenous MEP pathway and the integrated mevalonate module (Rs265-MVA) is compared with the three biological replicates of the knockout strains exclusively relying on the orthogonal MVA module (Rs265-MVA-*Δdxr* #5, 6 and 7). For all the strains, the yields were compared between strains relying exclusively on the integrated MVA module (pBB-*ads*, light blue) and others expressing additional MVA copies on a multicopy plasmid (pBBR-MVA-*ads*, dark blue). The error bars represent the standard deviations of biological triplicates. Significant differences are marked by either one or two asterisks (*$P < 0.05$, **$P < 0.01$). They were evaluated by comparing the set of replicates for the mutants Rs265-MVA-*Δdxr* to the replicates obtained by the Rs265-MVA strain by means of Student's *t*-test.

was inactivated, resulting in a twofold higher yield on glucose compared with the strain where the MEP pathway was still active. Therefore, this work is an example of the power of independent pathway substitutions for biotechnological optimization strategies, which holds potential for the generation of novel types of deregulated cell factories.

Experimental procedures

Strains, preculturing and culturing

The strains and plasmids used are listed in Table S1. The strain Rs265 was kindly provided by Isobionics BV. Unless specified, all *R. sphaeroides* cultivations were performed using Sistrom's minimal medium (SMM), containing: 3 g l^{-1} glucose, 3.48 g l^{-1} KH_2PO_4, 1.0 g l^{-1} NH_4Cl, 0.1 g l^{-1} glutamic acid, 0.04 g l^{-1} L-aspartic acid, 0.5 g l^{-1} NaCl, 0.02 g l^{-1} nitrilotriacetic acid, 0.3 g l^{-1} $MgSO_4·7H_2O$, 0.00334 g l^{-1} $CaCl_2·2H_2O$, 0.002 g l^{-1} $FeSO_4·7H_2O$, 0.0002 g l^{-1} $(NH_4)_6Mo_7O_{24}$. Trace elements were added 0.01 % v/v from a stock solution containing: 17.65 g l^{-1} disodium EDTA, 109.5 g l^{-1}

$ZnSO_4·7H_2O$, 50 g l^{-1} $FeSO_4·7H_2O$, 15.4 g l^{-1} $MnSO_4·7H_2O$, 3.92 g l^{-1} $CuSO_4$ ·5H_2O, 2.48 g l^{-1} Co$(NO_3)_2·6H_2O$, 0.114 g l^{-1} H_3BO_3. Vitamins were added 0.01 % v/v from a stock containing: 10 g l^{-1} nicotinic acid, 5 g l^{-1} thiamine HCl, 0.1 g l^{-1} biotin.

Preculturing of the strains started by their passage from glycerol stocks to LB plates supplemented with kanamycin 50 μg ml^{-1} and incubated at 30°C. After 48-72 h, once colonies were visible on the plates, they were transferred to Greiner tubes containing 5 ml liquid LB medium and kanamycin (50 μg ml^{-1}). The tubes were incubated for 24 h at 30°C and 250 rpm. Subsequently, an aliquot of 500 μl was transferred to a 250 ml Erlenmeyer flask containing 25 ml of SMM. Accordingly, incubation of the flasks at 30°C and 250 rpm were followed. After 16–20 h, the strains were diluted to an initial OD_{600} of 0.1 in 50 ml fresh SMM. When necessary, 10% v/v of dodecane was added to the aqueous phase.

Genomic integration of the mevalonate pathway

Genome editing of *R. sphaeroides* was performing using RÄ medium, which contained: 3 g l^{-1} malic acid (as only carbon source), 0.2 g l^{-1} $MgSO_4·7H_2O$, 1.2 g l^{-1} $(NH_4)_2SO_4$, 0.07 g l^{-1} $CaCl_2·2H_2O$, 1.5 ml of microelements stock solution, 2 ml of vitamin stock solution and 5 ml of phosphate buffer. In case of RÄ agar medium, 15 g l^{-1} agar was added. The microelements solution contained the following: 0.5 g l^{-1} Fe(II)-Citrate, 0.02 g l^{-1} $MnCl_2·4H_2O$, 0.005 g l^{-1} $ZnCl_2$, 0.0025 g l^{-1} KBr, 0.0025 g l^{-1} KI, 0.0023 g l^{-1} $CuSO_4·5H_2O$, 0.041 g l^{-1} Na_2MoO, 0.005 g l^{-1} $CoCl2·6H_2O$, 0.0005 g l^{-1} $SnCl_2·2H_2O$, 0.0006 g l^{-1} $BaCl_2·2H_2O$, 0.031 g l^{-1} AlCl, 0.41 g l^{-1} H_3BO, 0.02 g l^{-1} EDTA. The vitamin solution contained the following: 0.2 g l^{-1} nicotinic acid, 0.4 g l^{-1} thiamine HCl, 0.008 g l^{-1} biotin, 0.2 g l^{-1} nicotinamide. The phosphate buffer contained 0.6 g l^{-1} KH_2PO_4 and 0.9 g l^{-1} K_2HPO_4.

The mevalonate operon from *P. zeaxanthinifaciens* was cloned from plasmid pBBR-MVA (Hümbelin *et al.*, 2002, 2015) into plasmid pUC18Not (Biomedal, Sevilla, Spain) using restriction enzymes EcoRI and SphI. From the resulting plasmid pUC18Not-MVA, the operon was taken out and cloned into pUT-Mini-Tn5-Sp/Sm (Biomedal, Sevilla, Spain) using restriction enzyme NotI, according to the manufacturer's instructions. Orientation of the MVA operon in pUT-Mini-Tn5-Sp/Sm was confirmed by SphI digestion, and by sequencing using primers Tn5-fw and Tn5-Re (Table S2). Two clones called pUT-Tn5-MVA#1 and #2, each of them with a different orientation of the insert, were selected.

pUT-Tn5-MVA#1 and #2 were introduced into *Escherichia coli* S17-1 λpir (Biomedal, Sevilla, Spain) and were selected on ampicillin (100 μg ml^{-1}) and spectinomycin

(50 μg ml^{-1}). For conjugation, Rs265 harbouring pBBR-CnVS plasmid (Beekwilder *et al.*, 2014) was grown at 30°C in liquid RÄ medium supplemented with kanamycin (50 μg ml^{-1}). *E. coli* S17-1 λpir with pUT-Tn5-MVA#1 and #2 were grown overnight at 37°C in LB medium with ampicillin (100 μg ml^{-1}) and spectinomycin (50 μg ml^{-1}). *R. sphaeroides* and *E. coli* cells were washed and mixed for conjugation according to standard procedures, co-incubated on filters and finally plated on RÄ agar with kanamycin (50 μg ml^{-1}) and spectinomycin (50 μg ml^{-1}). Resulting colonies were purified on selective RS102 medium by re-streaking and were further selected by colony PCR, for the presence of mevalonate pathway (primers mvaA fw/re; mvd fw/re), CnVS (cnvs-fw/re) and Rhodobacter DNA (Rs-rps1 fw/re), and the absence of transposase (tnp-fw/re), to confirm integration of the MVA in the genome and absence of the plasmid. Thus, three independent lines of Rs265-MEV + pBBR-CnVS (#5, #6 and #7) were selected.

Plasmid assembly for deletion of dxr

All the primers used in this work are listed in the Table S2. For designing *dxr* deletion, the recently developed CRISPR-Cas9 toolbox for *R. sphaeroides* (Mougiakos *et al.*, 2019) was used. The plasmids used harboured the information for genomic *dxr* removal by homologous recombination (HR) and subsequent counter-selection via Cas9 targeting on the *wild-type* genomic copy of *dxr*. Assembly of the plasmid was performed by five-fragment HiFi Assembly (New England Biolabs, USA) as previously described (Mougiakos *et al.*, 2019). The non-targeting pBBR_Cas9_NT plasmid was used for amplification of the backbone with the primers P302/P303. Moreover, it was also used for amplifying the harmonized *spCas9* amplicon including the lacI promoter upstream to the coding sequence, while downstream contained the sgRNA module with the targeting spacer as overhang. Two spacers were used for targeting *dxr*; therefore, two variants of this amplicon were generated with the primers sets P301/P403 and P301/P407 for sp1 and sp2 respectively. The third amplicon generated using pBBR_Cas9_NT as template was obtained by using the complementary sequence of the spacers as overhang, and amplified a short fragment until the insertion point of the flanking sites for HR. Hence, since two spacers were used, the two amplicons were generated with the primers sets P304/P404 and P304/P408. The remaining two fragments included the flanking sites for HR. These two 1 kb fragments were designed for completely removing the *dxr* coding sequence (1185 bp). They were amplified from *R. sphaeroides* genomic DNA using the primers P399/P400 and P401/P402 and contained overhangs in their primers for assembly

of the plasmids pBBR_Cas9_Δ*dxr*_sp1 and pBBR_Cas9_Δ*dxr*_sp2.

Deletion of dxr for endogenous MEP inactivation

The two *dxr* targeting plasmids pBBR_Cas9_Δ*dxr*_sp1 and pBBR_Cas9_Δ*dxr*_sp2 were transferred to *R. sphaeroides* containing the integrated MVA pathway by conjugation as previously described (Mougiakos *et al.*, 2019). Conjugants were transferred to RÄ plates supplemented with kanamycin 50 μg ml^{-1}. Genomic DNA screening for presence of mutants was done by using the primers P437/P438. Additional colony PCRs for determining latent *dxr* copies were done with the primers P469/P471 and P468/P470. Validation of Δ*dxr* by colony PCR screening was followed by sequencing using the primers P455 and P456 for confirming *dxr* deletion from the genomic locus. Mutants were cured from the targeting plasmid by several passages in RÄ plates (kanamycin free). As control, each colony was additionally transferred in parallel to RÄ plates supplemented with kanamycin 50 μg ml^{-1}. Once the loss of antibiotic resistance was observed on plates supplemented with kanamycin, the plasmid removal was confirmed by PCR using the primers P368/P369, which amplify part of the coding sequence of the *spCas9* sequence. Δ*dxr* colonies were therefore conjugated with *E. coli* S17-1 λpir harbouring the pBBR-*ads* or pBBR-MVA-*ads* plasmids.

Growth and production assays

Quantitative physiological data on the strains were obtained by incubating the cultures with an initial OD$_{600}$ of 0.1 in 250 ml Erlenmeyer flasks containing 45 ml of SMM and 5 ml of dodecane. The medium was supplemented with kanamycin (50 μg ml^{-1}) for maintaining the pBBR-*ads* or pBBR-MVA-*ads* plasmid. The flasks were incubated at 30°C and 250 rpm. Growth was followed for the first 12 h for determining the growth (following OD) and glucose consumption rates (using YSI 2950 from Shimadzu). After 24 h, the cultivations were stopped, and the cultures were collected by centrifugation of the whole cultivation broth at 4255 *g* for 15 min. From the dodecane layer, amorphadiene concentrations were determined using a GC-FID 7890A from Agilent as previously described (Orsi *et al.*, 2019). From the aqueous phase, the residual glucose concentrations were measured using YSI 2950 from Shimadzu. The pellet was resuspended in MilliQ water to its original volume, and the biomass concentration at the end of the cultivation was calculated by measuring the total nitrogen in the suspension using a Total Organic Carbon analyzer (TOC-L) from Shimadzu.

^{13}C glucose cultivation

Cultivation was performed in 10 ml Erlenmeyer flasks containing 1.8 ml of SMM with 100% labelled [4-^{13}C]glucose (Sigma Aldrich) at a concentration of 3 g l^{-1}. 200 μl of dodecane was added, and the initial OD_{600} was 0.1. Incubations lasted for 24 h at 30°C and 250 rpm. At the end of the cultivation, the content of the flask was transferred to a 2 ml Eppendorf tube, and centrifugation at 14 000 g for 1 min followed. Then, the dodecane layer was collected and analysed by GC-MS. Chemical analysis was performed on an Agilent 7890A gas chromatograph connected to a 5975C mass selective Triple-Axis Detector (Agilent Technologies, USA). For quantification of amorphadiene, each sample was injected at 250°C in split-less mode on a ZB-5MS column (Zebron, Phenomenex, 30 m x 250 mm x 0.25 mm film thickness) with 5 m guard column, with a constant flow of helium at 1 ml min^{-1}. The oven was programmed for 1 min at 45°C, then ramped at 10°C min^{-1} to 300°C and kept as such for 5 min with a solvent delay of 12.5 min, for a final run time of 31.5 min.^{13}C atoms incorporation was determined analysing the increase in m/z values in the pool of secreted amorphadiene. As reference, the original m/z of 204 for amorphadiene was used.

Determination of endogenous terpenoids

For determination of the endogenous *R. sphaeroides* terpenoids, cultivation of the microorganisms was performed in 50 ml of SMM in a 250 ml Erlenmeyer flask. The cultivation started with an initial OD_{600} of 0.1, and lasted for 24 h at 30°C with 250 rpm. At the end of the cultivation, two aliquots of 10 ml of culture were centrifuged for 15 min at 4255 g. The first pellet was resuspended in MilliQ, and its nitrogen content was analysed by TOC-L from Shimadzu for active biomass determination. The second pellet was freeze-dried and further analysed for endogenous terpenoids determination. 10 mg of freeze-dried material was extracted by adding 2.5 ml of methanol with 0.1% butylhydroxytoluene (BHT), followed by addition of 2.5 ml of 50 mM Tris (pH = 7.5) + 1 M NaCl and 2 ml of chloroform + 0.1% BHT. After centrifugation, the chloroform phase was collected, and chloroform was aspired under a nitrogen flow. The pellet was dissolved in 100 μl ethylacetate + 0.1% BHT and analysed on HPLC as described previously (Beekwilder *et al.*, 2008). Compounds were identified based on absorption spectra, as already described (Lin *et al.*, 2014), and by comparison to original standards.

Conflict of interest

The authors declare no competing financial interests.

Authors' contributions

EO, JB and RW designed the work. EO, JB, DvG and AvH conducted, analysed and interpreted the experiments. EO and JB drafted and wrote the manuscript. All authors read and approved the final manuscript.

References

Ajikumar, P.K., Tyo, K., Carlsen, S., Mucha, O., Phon, T.H., and Stephanopoulos, G. (2008) Terpenoids: opportunities for biosynthesis of natural product drugs using engineered microorganisms. *Mol Pharm* **5:** 167–190.

Ajikumar, P.K., Xiao, W.H., Tyo, K.E.J., Wang, Y., Simeon, F., Leonard, E., *et al.* (2010) Isoprenoid pathway optimization for Taxol precursor overproduction in *Escherichia coli. Science (80-)* **330:** 70–74.

Beekwilder, J., van der Meer, I.M., Simic, A., Uitdewilligen, J., van Arkel, J., de Vos, R.C.H., *et al.* (2008) Metabolism of carotenoids and apocarotenoids during ripening of raspberry fruit. *Biofactors* **34:** 57–66.

Beekwilder, J., van Houwelingen, A., Cankar, K., van Dijk, A.D.J., de Jong, R.M., Stoopen, G., *et al.* (2014) Valencene synthase from the heartwood of Nootka cypress (*Callitropsis nootkatensis*) for biotechnological production of valencene. *Plant Biotechnol J* **12:** 174–182.

Benner, S.A., and Sismour, A.M. (2005) Synthetic biology. *Nat Rev Genet* **6:** 533–543.

Bentley, F.K., Zurbriggen, A., and Melis, A. (2014) Heterologous expression of the mevalonic acid pathway in cyanobacteria enhances endogenous carbon partitioning to isoprene. *Mol Plant* **7:** 71–86.

Bonacci, W., Teng, P.K., Afonso, B., Niederholtmeyer, H., Grob, P., Silver, P.A., and Savage, D.F. (2012) Modularity of a carbon-fixing protein organelle. *Proc Natl Acad Sci USA* **109:** 478–483.

Carlsen, S., Ajikumar, P.K., Formenti, L.R., Zhou, K., Phon, T.H., Nielsen, M.L., *et al.* (2013) Heterologous expression and characterization of bacterial 2-C-methyl-d-erythritol-4-phosphate pathway in *Saccharomyces cerevisiae. Appl Microbiol Biotechnol* **97:** 5753–5769.

Chatzivasileiou, A.O., Ward, V., Edgar, S.M., and Stephanopoulos, G. (2019) Two-step pathway for isoprenoid synthesis. *Proc Natl Acad Sci USA* **116:** 506–511.

Erb, T.J., Evans, B.S., Cho, K., Warlick, B.P., Sriram, J., Wood, B.M.K., *et al.* (2012) A RubisCO-like protein links

SAM metabolism with isoprenoid biosynthesis. *Nat Chem Biol* **8:** 926–932.

Flamholz, A., Noor, E., Bar-Even, A., and Milo, R. (2012) EQuilibrator – The biochemical thermodynamics calculator. *Nucleic Acids Res* **40:** 770–775.

Grünler, J., Ericsson, J., and Dallner, G. (1994) Branch-point reactions in the biosynthesis of cholesterol, dolichol, ubiquinone and prenylated proteins. *Biochim Biophys Acta (BBA)/Lipids Lipid Metab* **1212:** 259–277.

Hümbelin, M., Thomas, A., Lin, J., Li, J., Jore, J., and Berry, A. (2002) Genetics of isoprenoid biosynthesis in *Paracoccus zeaxanthinifaciens*. *Gene* **297:** 129–139.

Hümbelin, M., Beekwilder, J., and Kierkels, J. G. T. (2015) *Rhodobacter for preparing terpenoids*. Patent no. WO2014014339A3.

Jiang, W., Qiao, J.B., Bentley, G.J., Liu, D., and Zhang, F. (2017) Modular pathway engineering for the microbial production of branched-chain fatty alcohols. *Biotechnol Biofuels* **10:** 1–15.

Kendig, C., and Eckdahl, T.T. (2017) Reengineering metaphysics: modularity, parthood, and evolvability in metabolic engineering. *Philos Theory, Pract Biol* **9:** 1–21.

Kirby, J., and Keasling, J.D. (2009) Biosynthesis of plant isoprenoids: perspectives for microbial engineering. *Annu Rev Plant Biol* **60:** 335–355.

Kirby, J., Nishimoto, M., Chow, R.W.N., Baidoo, E.E.K., Wang, G., Martin, J., *et al.* (2015) Enhancing Terpene yield from sugars via novel routes to 1-deoxy-D-xylose 5-phosphate. *Appl Environ Microbiol* **81:** 130–138.

Kirby, J., Dietzel, K.L., Wichmann, G., Chan, R., Antipov, E., Moss, N., *et al.* (2016) Engineering a functional 1-deoxy-D-xylulose 5-phosphate (DXP) pathway in *Saccharomyces cerevisiae*. *Metab Eng* **38:** 494–503.

Liao, J.C., Mi, L., Pontrelli, S., and Luo, S. (2016) Fuelling the future: microbial engineering for the production of sustainable biofuels. *Nat Rev Microbiol* **14:** 288–304.

Lin, Z., Cui, X., Zhao, C., Yang, S., and Imhoff, J.F. (2014) Pigments accumulation via light and oxygen in *Rhodobacter capsulatus* strain XJ-1 isolated from saline soil. *J Basic Microbiol* **54:** 828–834.

Liu, C.C., Jewett, M.C., Chin, J.W., and Voigt, C.A. (2018) Toward an orthogonal central dogma. *Nat Chem Biol* **14:** 103–106.

Loiseau, L., Gerez, C., Bekker, M., Ollagnier-De Choudens, S., Py, B., Sanakis, Y., *et al.* (2007) ErpA, an iron-sulfur (Fe-S) protein of the A-type essential for respiratory metabolism in *Escherichia coli*. *Proc Natl Acad Sci USA* **104:** 13626–13631.

Lombard, J., and Moreira, D. (2011) Origins and early evolution of the mevalonate pathway of isoprenoid biosynthesis in the three domains of life. *Mol Biol Evol* **28:** 87–99.

Lu, W., Ye, L., Lv, X., Xie, W., Gu, J., Chen, Z., *et al.* (2015) Identification and elimination of metabolic bottlenecks in the quinone modification pathway for enhanced coenzyme Q 10 production in *Rhodobacter sphaeroides*. *Metab Eng* **29:** 208–216.

Mewalal, R., Rai, D.K., Kainer, D., Chen, F., Külheim, C., Peter, G.F., and Tuskan, G.A. (2016) Plant-derived terpenes: a feedstock for specialty biofuels. *Trends Biotechnol* **35:** 227–240.

Mougiakos, I., Orsi, E., Ghiffari, M.R., De Maria, A., Post, W., Adiego-Perez, B., *et al.* (2019) Efficient Cas9-based genome editing of *Rhodobacter sphaeroides* for metabolic engineering. *Microb Cell Fact* **18:** 1–13.

Niu, F.X., Lu, Q., Bu, Y.F., and Liu, J.Z. (2017) Metabolic engineering for the microbial production of isoprenoids: carotenoids and isoprenoid-based biofuels. *Synth Syst Biotechnol* **2:** 167–175.

Orsi, E., Folch, P.L., Monje-López, V.T., Fernhout, B.M., Turcato, A., Kengen, S.W.M., *et al.* (2019) Characterization of heterotrophic growth and sesquiterpene production by *Rhodobacter sphaeroides* on a defined medium. *J Ind Microbiol Biotechnol* **46:** 1179–1190.

Orsi, E., Beekwilder, J., Peek, S., Eggink, G., Kengen, S.W.M., and Weusthuis, R.A. (2020) Metabolic flux ratio analysis by parallel biosynthesis in *Rhodobacter sphaeroides* ^{13}C labeling of isoprenoid. *Metab Eng* **57:** 228–238.

Partow, S., Siewers, V., Daviet, L., Schalk, M., and Nielsen, J. (2012) Reconstruction and evaluation of the synthetic bacterial MEP pathway in *Saccharomyces cerevisiae*. *PLoS One* **7:** 1–12.

Peralta-Yahya, P.P., Zhang, F., Cardayre, D.S.B., and Keasling, J.D. (2012) Microbial engineering for the production of advanced biofuels. *Nature* **488:** 320–328.

Puan, K.J., Wang, H., Dairi, T., Kuzuyama, T., and Morita, C.T. (2005) *fldA* is an essential gene required in the 2-C-methyl-D-erythritol 4-phosphate pathway for isoprenoid biosynthesis. *FEBS Lett* **579:** 3802–3806.

Schempp, F.M., Drummond, L., Buchhaupt, M., and Schrader, J. (2017) Microbial cell factories for the production of terpenoid flavor and fragrance compounds. *J Agric Food Chem* **66:** 2247–2258.

Stephanopoulos, G. (2012) Synthetic biology and metabolic engineering. *ACS Synth Biol* **1:** 514–525.

Vranová, E., Coman, D., and Gruissem, W. (2013) Network analysis of the MVA and MEP pathways for isoprenoid synthesis. *Annu Rev Plant Biol* **64:** 665–700.

Withers, S.T., and Keasling, J.D. (2007) Biosynthesis and engineering of isoprenoid small molecules. *Appl Microbiol Biotechnol* **73:** 980–990.

Wu, J., Liu, P., Fan, Y., Bao, H., Du, G., Zhou, J., and Chen, J. (2013) Multivariate modular metabolic engineering of *Escherichia coli* to produce resveratrol from l-tyrosine. *J Biotechnol* **167:** 404–411.

Zhou, K., Qiao, K., Edgar, S., and Stephanopoulos, G. (2015) Distributing a metabolic pathway among a microbial consortium enhances production of natural products. *Nat Biotechnol* **33:** 377–383.

Zurbriggen, A., Kirst, H., and Melis, A. (2012) Isoprene production via the mevalonic acid pathway in *Escherichia coli* (Bacteria). *Bioenergy Res* **5:** 814–828.

Supporting information

Additional supporting information may be found online in the Supporting Information section at the end of the article.

Fig. S1. Plasmids map of pBBR-Cas9-dxr-HR plasmid. In this map, the spacer sp1 is included.

Fig. S2. Genetic evidence of endogenous MEP pathway inactivation by deletion of *dxr*. (A) Colony PCR using the primer set P437/P438, annealing outside the flanking sites employed for homologous recombination. The expected fragment size is 3388 bp for the wild-type, while it is 2200 bp for Δ*dxr*. (B) Colony PCR for detecting latent wild-type *dxr* copies within the genome. This amplification aims to identify possible copies of *dxr* which might have escaped the Cas9 counter-selection and might have not been detected by the primer set P437/P438. The two primer sets P468/P470 and P469/P471 amplify fragments of *dxr* at the 5' and 3'ends, respectively. Only in case of *dxr* presence, the PCR product would result in the creation of two bands of the length of 2341 and 1721 bp.

Fig. S3. Growth rates profile for the strains containing the pBBR-ads plasmid.

Fig. S4. Growth rates profile for the strains containing the pBBR-MVA-ads plasmid.

Table S1. List of strains and plasmids used in this study.

Table S2. Primers used in this work. See methods section in the manuscript for details about the primers combinations used.

Table S3. Biological functions of the genes belonging to the *dxr* operon.

Table S4. Spacers used for targeting *dxr*.

Table S5. Overview of the standard Gibbs free energies of the different enzymatic reactions for the two isoprenoid biosynthetic routes. Values are calculated using EQuilibrator (Flamholz et al., 2012).

Table S6. Efficiencies of *dxr* deletion via spacers sp1 and sp2.

Table S7. Glucose consumption rates in strains Rs265-MVA and Rs265-MVA-Δ*dxr*.